

# Hole-spin qubits in germanium beyond the single-particle regime

Andrea Secchi<sup>1,\*</sup>, Gaia Forghieri<sup>1,2</sup>, Paolo Bordone<sup>1,2</sup>, Daniel Loss<sup>3,4,5,6</sup>, Stefano Bosco<sup>7</sup>, Filippo Troiani<sup>1</sup>

<sup>1</sup>*Centro S3, CNR-Istituto Nanoscienze, 41125 Modena, Italy*

<sup>2</sup>*Dipartimento di Scienze Fisiche, Informatiche e Matematiche,*

*Università degli Studi di Modena e Reggio Emilia, Via G. Campi 213/a, 41125 Modena, Italy*

<sup>3</sup>*Department of Physics, University of Basel, Klingelbergstrasse 82, CH-4056 Basel, Switzerland*

<sup>4</sup>*Physics Department, King Fahd University of Petroleum and Minerals, 31261, Dhahran, Saudi Arabia*

<sup>5</sup>*Quantum Center, KFUPM, Dhahran, Saudi Arabia*

<sup>6</sup>*RDIA Chair in Quantum Computing*

<sup>7</sup>*QuTech and Kavli Institute of Nanoscience, Delft University of Technology, Delft, The Netherlands*

(Dated: March 3, 2026)

The intense simulation efforts on hole-spin qubits in germanium have so far focused primarily on singly occupied quantum dots. Here, we theoretically investigate three-hole qubits in germanium and demonstrate that their performance can rival that of single-hole qubits in both strained and unstrained systems. In particular, we find that — in the widely used quasi-circular geometry — a three-hole qubit encoding can yield enhancements of the Rabi frequencies of up to two orders of magnitude and a large advantage also in terms of quality factors.

*Introduction.* Spin qubits in semiconductor quantum dots (QDs) are promising competitors for the implementation of quantum computers [1–15]. In particular, the low natural abundance of magnetic nuclei, combined with the possibility of isotopic purification, grants long coherence times for spins in silicon (Si) and germanium (Ge) [2, 3, 16–23]. In these systems, high fidelities have been achieved in all fundamental computational tasks, from one- and two-qubit gates [24–29] to initialization and readout [30–32]. Besides, the advanced fabrication techniques and integration circuitry provide excellent scalability prospects and allow a high degree of control even at relatively high temperatures [11, 14, 15, 18, 33–36].

In contrast to electrons, holes in Ge have no valley degeneracy and are characterized by strong spin-orbit coupling (SOC) which allows for all-electric manipulation [21, 37–48]. In addition, due to their  $p$ -orbital character, they are less susceptible than electrons to the hyperfine interaction [6, 49–51]. Finally, the characteristic properties of the hole-spin qubit, including the  $g$  tensor and the Rabi frequencies, are electrically tunable [35, 52]. This results from the susceptibility to the electrostatic environment of the mixing between heavy-hole (HH), light-hole (LH), and split-off (SO) bands [8, 12, 39, 53–58].

The vast majority of the literature on hole-spin qubits focuses on single-particle encodings. Multiple holes, localized in singly-occupied QDs, have also been considered for alternative qubit encodings [10, 20, 59–64]. On the other hand, an odd number of holes in a *single* QD enables qubit encodings and manipulation schemes analogous to those implemented in the single-particle case [65–67]. Such a multi-hole single-dot qubit has a twofold interest. First, from an experimental point of view, it relaxes the stringent requirement of achieving the single-occupation regime. Second, and most importantly, it might result in larger and more local couplings to the control gates and, ultimately, in improved figures of merit

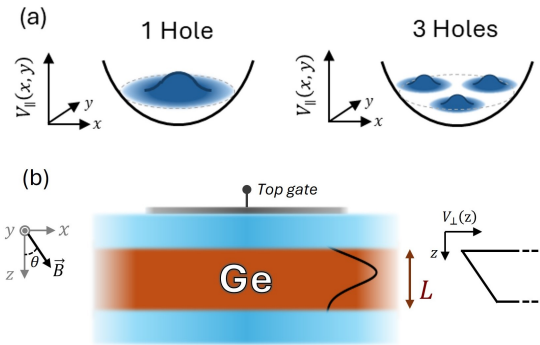


FIG. 1. (a) Pictorial representation of a single-hole state (left) and a three-hole state (right) in a QD elongated along the  $x$  direction. (b) Schematic view of a MOS device, where the Ge channel has a width  $L$  along the  $z$  direction. The bias applied to the metal top gate determines the in-plane confining potential  $V_{\parallel}$  and the linear (in  $z$ ) contribution in the out-of-plane confining potential  $V_{\perp}$ .

[68]. However, despite their past and recent occurrence in experiments [11, 12, 44, 45, 69, 70], few-particle effects in semiconductor hole-spin qubits remain relatively unexplored at the theoretical level.

In this Letter, we provide a theoretical study of multi-hole qubits in Ge QDs, implemented in unstrained MOS-like devices and in Ge/Si<sub>1-x</sub>Ge<sub>x</sub> heterostructures (Fig. 1). Focusing on the case of three holes, we show that the main figures of merit are always at least comparable to those obtained for single holes, and significantly improved in specific regimes. More specifically, the Rabi frequency of the three-hole qubit (THQ) is shown to exceed that of a single-hole qubit (SHQ) by up to two orders of magnitude in quasi-circular QDs. This occurs without a significant modification of the  $g$  factor or loss of the qubit coherence under charge noise. As the comparison of the fully interacting THQ with its noninteracting counterpart shows,

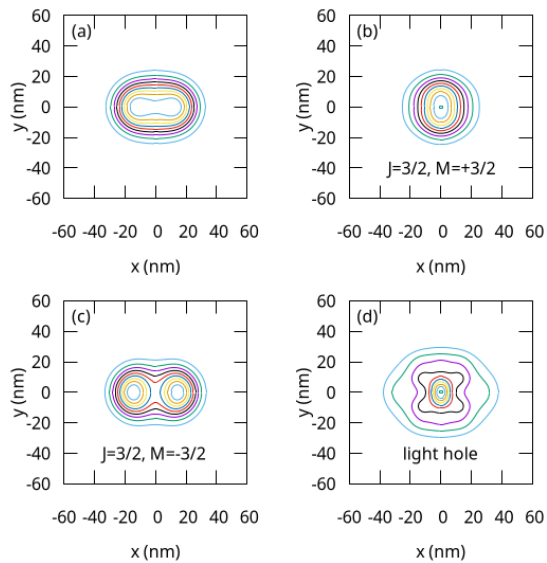


FIG. 2. In-plane particle distribution  $N_z(x, y)$  for the ground state  $|\Phi_0\rangle$  of the three-hole system, obtained by integrating the particle density  $n(\mathbf{r})$  along the  $z$  direction. The four panels display: (a) the function  $N_z(x, y)$ ; (b,c) the heavy-hole contributions; (d) the sum of the two light-hole contributions. All the plotted functions are normalized to 1, the isolines correspond to values that are multiples of 0.1. The values of the parameters are:  $\hbar\omega_x = 5$  meV,  $\hbar\omega_y = 6$  meV,  $B = 0.05$  T and  $\theta = 0$  (parallel field orientation).

this gain is caused, for the largest part, by the occupation of the excited orbitals dictated by the Pauli principle, the hole-hole interaction giving a quantitatively smaller (albeit far from negligible) contribution in that regime. Strain changes the absolute values of the manipulation frequencies, but does not substantially affect the relative performances of the single- and multi-hole qubits.

*Quantum-dot model.* Single-hole states are derived through the numerical diagonalization of the 6-band  $\mathbf{k}\cdot\mathbf{p}$  Hamiltonian resulting from the Luttinger-Kohn (LK) envelope-function approach [53, 71–73]. The 6 bands needed to describe single-hole states in Ge close to the top of the valence band form a  $J = 3/2$  quadruplet and a  $J = 1/2$  doublet, with  $J$  being the total atomic angular momentum associated with the Bloch states at the  $\Gamma$  point. These two multiplets are split at  $\Gamma$  by spin-orbit coupling (SOC), which induces a gap  $\Delta_{\text{SO}} = 290$  meV. The  $J = 3/2$  quadruplet, degenerate at  $\Gamma$ , is split into the HH ( $|M| = 3/2$ ) and the LH ( $|M| = 1/2$ ) doublets at finite  $k$ . The band structure around the  $\Gamma$  point is determined by the LK parameters, which, for Ge, are:  $\gamma_1 = 13.38$ ,  $\gamma_2 = 4.24$  and  $\gamma_3 = 5.69$ . The reference frame, specified by the unit vectors  $\mathbf{u}_x$ ,  $\mathbf{u}_y$ , and  $\mathbf{u}_z$ , is defined with respect to the crystallographic axes as follows:  $\mathbf{u}_x \parallel [110]$ ,  $\mathbf{u}_y \parallel [\bar{1}10]$ ,  $\mathbf{u}_z \parallel [001]$ .

The confining potential that defines the dot model varies smoothly with respect to the unit-cell scale, and is

specifically given by

$$V_{\text{conf}}(\mathbf{r}) = \frac{1}{2} \frac{m_0}{\gamma_1} (\omega_x^2 x^2 + \omega_y^2 y^2) + V_{\perp}(z). \quad (1)$$

Here,  $m_0$  is the free-electron mass, while  $\hbar\omega_y$  (set to 6 meV) and  $\hbar\omega_x$  (from 3 to 5.5 meV) are the characteristic energy scales associated with the anisotropic harmonic confinement in the  $xy$  plane. The out-of-plane confinement defines a quantum well, resulting from the band offset between Ge and the barrier material:

$$V_{\perp}(z) = W + \frac{W}{2} \sum_{\xi=\pm 1} \tanh \left[ \xi \frac{z}{s} - \frac{(1+\xi)L}{2s} \right] + e_{\perp} z. \quad (2)$$

Here,  $L = 10$  nm is the well width,  $W$  is the barrier height, and  $s = 0.02$  nm a smoothing factor. The dc electric field  $e_{\perp} = 1$  meV/nm, possibly associated to a top gate voltage, is attractive for holes.

The coupling to the magnetic field is introduced into the single-hole Hamiltonian through the Zeeman-Bloch term and the Peierls substitution [35, 52], with the electromagnetic vector potential expressed in the Coulomb gauge. The magnetic field is given in polar form,  $\mathbf{B} \equiv B(\sin\theta \cos\phi, \sin\theta \sin\phi, \cos\theta)$ , with  $B = 0.05$  T,  $\phi = 45^\circ$ , and a variable polar angle  $\theta$ .

The few-particle (three-hole) eigenstates are computed by diagonalizing the interacting Hamiltonian, within the full configuration interaction approach [74, 75]. The three-hole Slater determinants are built from a set of 64 single-particle states, which ensures the convergence of the relevant quantities. Further details on the method are provided in the Supplemental Material (SM) [76].

*Single- and three-hole spin qubits.* The magnetic field breaks the Kramers degeneracy within the ground doublet, and induces the energy splitting  $\Delta_{10}^{(k)}$  between the states  $|0^{(k)}\rangle$  and  $|1^{(k)}\rangle$ , which define the SHQ ( $k = 1$ ) and the THQ ( $k = 3$ ). This splitting can equivalently be expressed in terms of the  $g$  factor  $g_{\theta}^{(k)} = \Delta_{10}^{(k)} / \mu_B B$ , which depends on the orientation of  $\mathbf{B}$  with respect to the  $z$  axis, defined by  $\theta$ .

QD1	$g_{\theta}^{(1)}$	$g_{\theta}^{(3)}$	$f_{R,x}^{(3)}$	$f_{R,y}^{(3)}$
$\theta = 0^\circ$	8.67	7.99 (6.25)	46.8 (239)	9.24 (27.3)
$\theta = 90^\circ$	0.121	0.0848 (0.104)	7.29 (3.93)	2.07 (0.0775)
QD2	$g_{\theta}^{(1)}$	$g_{\theta}^{(3)}$	$f_{R,x}^{(3)}$	$f_{R,y}^{(3)}$
$\theta = 0^\circ$	8.00	4.88 (4.34)	394 (322)	313 (175)
$\theta = 90^\circ$	0.114	0.220 (0.321)	27.1 (23.9)	11.3 (2.04)

TABLE I. Values of the  $g$  factors and of the Rabi frequencies (expressed in MHz) for the unstrained single- and three-hole qubits, for  $\hbar\omega_y = 6$  meV,  $B = 0.05$  T, and  $|\delta\mathbf{E}_R| = 1$  mV/nm. The value of  $\hbar\omega_x$  is 3 and 5.5 meV for QD1 and QD2, respectively. In parentheses we report the Rabi frequencies of the noninteracting THQ.

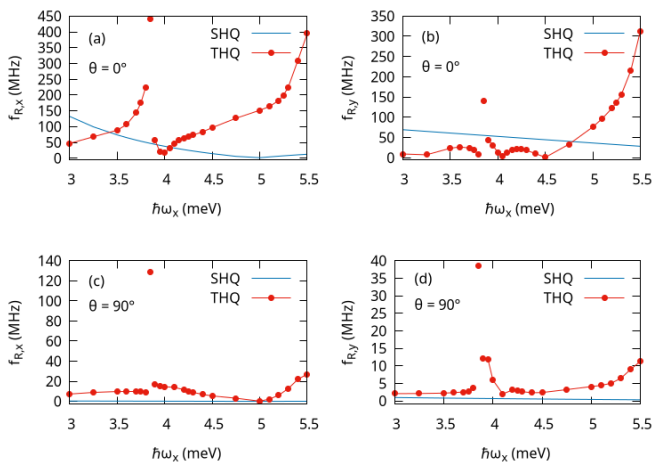


FIG. 3. Rabi frequencies  $f_{R,\alpha}^{(n)}$  of the  $n$ -hole qubit as functions of  $\hbar\omega_x$ , with  $n = 1$  (red curves) and  $n = 3$  (blue symbols), when the oscillating electric field (of amplitude  $|\delta\mathbf{E}_R| = 1$  mV/nm) is oriented along the  $x$  (a, c) or  $y$  direction (b, d). The magnetic field amplitude is  $|\mathbf{B}| = 0.05$  T; its direction is given by  $\theta = 0^\circ$  (a, b) or  $\theta = 90^\circ$  (c, d), with  $\phi = 45^\circ$ .

The qubit manipulation is performed by applying an oscillating electric field  $\delta\mathbf{E}(t) = \delta\mathbf{E}_R \cos(\omega t)$ , in resonance with the Larmor frequency ( $\omega = 2\pi f_L$ ). The resulting Rabi frequency is given by:

$$f_R^{(k)} = \frac{e}{\hbar} |\delta\mathbf{E}_R \cdot \langle 0^{(k)} | \hat{\mathbf{r}} | 1^{(k)} \rangle|, \quad (3)$$

where  $\hat{\mathbf{r}}$  is the hole position operator, and  $|\delta\mathbf{E}_R| = 1$  mV/nm is the amplitude of the spatially homogeneous oscillating electric field.

As a first means to characterize the three-hole ground state  $|0^{(3)}\rangle$ , we compute the particle density

$$n(\mathbf{r}) = \sum_{\beta} n_{\beta}(\mathbf{r}) = \sum_{\beta} \langle 0^{(3)} | \hat{\psi}_{\beta}^{\dagger}(\mathbf{r}) \hat{\psi}_{\beta}(\mathbf{r}) | 0^{(3)} \rangle, \quad (4)$$

where  $\beta$  runs over the six hole bands and the field operator  $\hat{\psi}_{\beta}(\mathbf{r})$  annihilates a hole belonging to the band  $\beta$  at the position  $\mathbf{r}$ . Being the particle density along the vertical direction weakly correlated with that in the planar directions [76], we focus on the in-plane particle distribution, represented by  $N_z(x, y) \equiv \int dz n(\mathbf{r})$  (Fig. 2). The three holes clearly display a linear arrangement along the weak-confinement direction ( $x$ ), characterized by the presence of three peaks [panel (a)], which become increasingly resolved for decreasing values of  $\omega_x$  [76]. Besides, the minority [ $M = +3/2$ , panel(b)] and majority [ $M = -3/2$ , panel(c)] HH components of  $N_z(x, y) \equiv \int dz n(\mathbf{r})$  are clearly related to the central and external peaks, respectively: the ground state of the THQ is thus characterized by an ‘‘antiferromagnetic’’ ordering in the pseudospin defined by the HH component ( $M = \pm 3/2$ ). The in-plane distribution of the LH components [panel (d)], whose weight represent less than 1% of the total, display markedly different features.

The comparison between single- and multi-hole qubit encodings is mainly defined in terms of the respective  $g$  factors and Rabi frequencies. Concerning the former ones, no significant difference is observed between SHQs and THQs. Both  $g^{(1)}$  and  $g^{(3)}$  are characterized by a weak dependence on the in-plane aspect ratio  $\omega_x/\omega_y$  of the dot, and by a dependence on  $\theta$  that, for  $|\theta - 90^\circ| \gg 1^\circ$ , is given by:  $g_{\theta}^{(k)} \approx g_{0^\circ}^{(k)} \cos \theta$ . This relation results from the strong  $g$  factor anisotropy ( $g_{0^\circ}^{(k)} \gg g_{90^\circ}^{(k)}$ ), which — in the case of the THQ — is significantly enhanced by the Coulomb interactions (see the absolute values and the comparison with the non-interacting three-hole states for the elongated and quasi-circular QDs in Table I).

While the  $g$  factors of the THQ and of the SHQ show a very similar dependence on the orientation of  $\mathbf{B}$ , the Rabi frequencies differ remarkably in the two cases (Fig. 3). In fact, for all the considered orientations of  $\mathbf{B}$  and of the oscillating electric field  $\delta\mathbf{E}_R$ , the Rabi frequency of the THQ displays a non-monotonic dependence on the dot aspect ratio ( $\omega_x$ ). Moreover, the  $f_{R,\alpha}^{(3)}$  are characterized by the presence of pronounced maxima, and by regions corresponding to a large enhancement with respect to the SHQ, mostly — but not exclusively — concentrated in the quasi-circular dot regime ( $\hbar\omega_x \gtrsim 5$  meV). Sharp peaks in the Rabi frequencies of the THQ show up at  $\hbar\omega_x \approx 3.8$  meV. These features correspond to, and are most likely related to, the presence of a narrow anticrossing between the first and second excited doublet [76].

The question arises as to whether these striking differences between the THQ and the SHQ are mainly due to Coulomb interaction or to the occupation of excited single-particle states, imposed by the Pauli principle [77]. In order to discriminate between these two cases, we compare the above values of the Rabi frequencies with those obtained for the noninteracting three-hole system ( $f_{R,\alpha}^{(k)}$ ). The difference between the two cases is always remarkable and shows that the values of the Rabi frequencies are strongly affected by the Coulomb interactions. Whether the Rabi frequencies of the THQ are larger or smaller than those of the noninteracting three-hole system de-

QD1	$f_{R,x}^{(1)}$	$f_{R,y}^{(1)}$	$\tau^{(1)}$	$f_{R,x}^{(3)}$	$f_{R,y}^{(3)}$	$\tau^{(3)}$
$\theta = 0^\circ$	57.5	27.0	5.78	23.0	5.30	5.92
$\theta = 90^\circ$	0.276	0.0804	1480	0.0941	0.157	1130
QD2	$f_{R,x}^{(1)}$	$f_{R,y}^{(1)}$	$\tau^{(1)}$	$f_{R,x}^{(3)}$	$f_{R,y}^{(3)}$	$\tau^{(3)}$
$\theta = 0^\circ$	4.48	10.7	5.93	63.7	33.9	4.50
$\theta = 90^\circ$	0.0223	0.0494	752	0.301	0.349	3690

TABLE II. Values of the Rabi frequencies (expressed in MHz) and of the dephasing time scales (in  $\mu\text{s}$ ) of the strained single- and three-hole qubits, for  $\hbar\omega_y = 6$  meV,  $B = 0.05$  T,  $|\delta\mathbf{E}_R| = 1$  mV/nm, and  $|\mathbf{E}_{\text{cn}}| = 10^{-2}$  mV/nm. The value of  $\hbar\omega_x$  is 3 and 5.5 meV for QD1 and QD2, respectively.

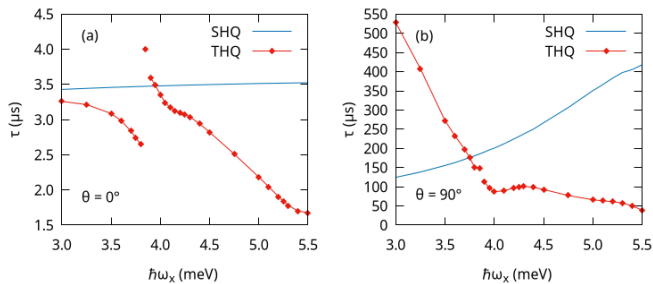


FIG. 4. Dephasing time scale  $\tau$  as a function of  $\hbar\omega_x$  (with  $\hbar\omega_y = 6$  meV), for a magnetic field of intensity  $B = 0.05$  T oriented (a) parallel ( $\theta = 0^\circ$ ) or (b) perpendicular ( $\theta = 90^\circ$ ) to the  $z$  axis. The charge-noise induced electric field is oriented along the  $z$  direction, with  $|\mathbf{E}_{\text{cn}}| = 10^{-2}$  mV/nm.

depends on the orientation of the magnetic field and on the degree of elongation of the QD (Table I).

*Qubit dephasing.* Random fluctuations in the energy gap  $\Delta_{10}$ , induced by charge noise, are generally regarded as the main source of decoherence for hole-spin qubits [2]. The dephasing time scale  $\tau$  can thus be defined as:

$$\frac{1}{\tau^{(k)}} \equiv \frac{e}{\hbar} \left| \mathbf{E}_{\text{cn}} \cdot \left( \langle 1^{(k)} | \hat{\mathbf{r}} | 1^{(k)} \rangle - \langle 0^{(k)} | \hat{\mathbf{r}} | 0^{(k)} \rangle \right) \right|. \quad (5)$$

Here,  $\mathbf{E}_{\text{cn}}$  is a characteristic value of the charge-noise induced electric field vector. If the field is spatially homogeneous throughout the QD region then, due to the symmetries of the confinement potential, the dominant contribution in  $1/\tau$  is the one related to the  $z$  component of  $\mathbf{E}_{\text{cn}}$ . As in the case of the Rabi frequencies, attention should be paid to the trends and to the comparison between single- and three-hole spin qubits, rather than to the absolute values of the dephasing time scale, which depend on the assumed value of the charge-noise induced electric field.

The differences between the values of  $\tau$  obtained in the single- and in the three-hole qubits are remarkable. Similarly to the case of the Rabi frequencies, the monotonic dependence of  $\tau$  on the dot aspect ratio ( $\omega_x$ ) that is obtained for the SHQ is replaced — in the case of the THQ — by a non-monotonic dependence, which varies qualitatively with the magnetic-field orientation (Fig. 4). In particular, we note that the dephasing time scale of the THQ is lower than that of the SHQ for a quasi-circular dot. However, the enhancement that the THQ allows in terms of Rabi frequency overcompensates such an effect, resulting in a higher value of a quality factor  $Q_x \equiv f_{R,x} \tau$  (see below). As for the Rabi frequencies, the region corresponding to  $\hbar\omega_x \approx 3.8$  meV is characterized by strong variations of  $\tau$ , which we attribute to the effect on the ground state doublet of the narrow anticrossing affecting the two lowest excited doublets [76].

*Effect of strain.* We hereafter investigate the effect of a homogeneous biaxial strain, such as the one that can result from the lattice mismatch in Ge/Si<sub>1-x</sub>Ge<sub>x</sub> het-

erostructures. The Hamiltonian term related to a small and homogeneous strain is derived, within the  $\mathbf{k} \cdot \mathbf{p}$  formalism, by the Bir-Pikus theory [78–80]. In particular, we consider a diagonal uniaxial strain tensor,  $\varepsilon_\beta^\alpha = \delta_\beta^\alpha \varepsilon_\alpha^\alpha$ , with  $\varepsilon_x^x = \varepsilon_y^y = \varepsilon_\parallel$  and  $\varepsilon_z^z = -2\varepsilon_\parallel C_{12}/C_{11}$ , (where  $C_{11} = 126$  GPa and  $C_{12} = 44$  GPa are the elastic constants of Ge [81]), and a typical Ge concentration  $x = 0.8$  in the alloy, for which the measured strain parameter is  $\varepsilon_\parallel = -0.0063$  [82].

The presence of strain significantly affects the values of the quantities considered so far. The strain increases the energy difference between the HH and LH components, enhancing the HH character of the single-hole ground state. This results in an increased  $g$ -factor anisotropy, both in the SHQ and in the THQ. As to the Rabi frequencies, their values are generally reduced by the presence of strain, to a similar extent for the SHQs and the THQs. However, the presence of biaxial strain also results in a systematic increase of  $\tau^{(1)}$  and  $\tau^{(3)}$ , as shown in Table II for the cases of the elongated and quasi-circular dots. Overall, the QD quality factor presents non-monotonic dependencies on the in-plane aspect ratio, with no general advantage or disadvantage resulting from the presence of strain (Fig. 5). On the other hand, the value of  $Q_x$  obtained for the THQ largely exceeds that of the SHQ (figure inset) in the quasi-circular geometry, both for the strained and for the unstrained dot. This shows that the advantage of the three-hole encoding in terms of Rabi frequency overcompensates the advantage of the SHQ at the level of dephasing time scale.

*Conclusions.* The various scenarios considered in this work consistently point to the fact that three-hole spin qubits in Ge perform better than their single-hole counterparts when the QD is close to the circular regime.

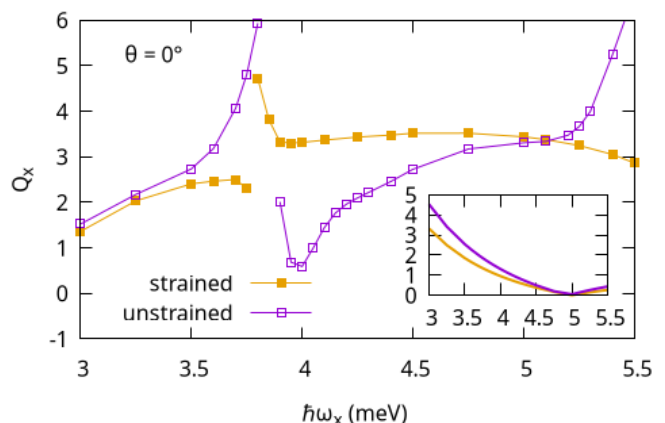


FIG. 5. Quality factor  $Q_x$  for the THQ as a function of  $\hbar\omega_x$  (with  $\hbar\omega_y = 6$  meV), for a magnetic field intensity  $B = 0.05$  T oriented out of plane (parallel to the  $z$  axis). Yellow and purple symbols correspond to the strained and to the unstrained dots, respectively. Inset:  $Q_x$  vs  $\hbar\omega_x$  for the SHQ, with the same units and the same color code as in the main plot.

In both cases, the largest Rabi frequencies associated to in-plane oscillating electric fields are obtained for magnetic fields oriented along the growth direction. Biaxial strain leads to an overall reduction of the Rabi frequencies, which is however balanced by a comparable increase in the characteristic dephasing time, resulting in no significant difference between strained and unstrained dots in terms of quality factor.

We are particularly grateful to Y.-M. Niquet for an insightful comment, and we thank the members of the Niquet, Veldhorst, Rimbach-Russ, and Scappucci groups for helpful discussions. We acknowledge the CINECA award under the IS CRA initiative, for the availability of high-performance computing resources and support (IsCb4-GERONIMO - HP10CG99PB). This work was funded by the Italian PNRR Project PE0000023-NQSTI and, as a part of NCCR SPIN, a National Centre of Competence in Research, by the Swiss National Science Foundation (grant number 225153). SB was also supported by the EU through the H2024 QLSI2 project and the Army Research Office under Award Number: W911NF-23-1-0110. DL acknowledges the Deanship of Research at KFUPM and the Quantum Center for the support received under Grant no. CUP25102 and no. INQC2500, respectively. The views and conclusions contained in this document are those of the authors and should not be interpreted as representing the official policies, either expressed or implied, of the Army Research Office or the U.S. Government. The U.S. Government is authorized to reproduce and distribute reprints for Government purposes notwithstanding any copyright notation herein.

---

\* [andrea.secchi@nano.cnr.it](mailto:andrea.secchi@nano.cnr.it)

- [1] D. Loss and D. P. DiVincenzo, Quantum computation with quantum dots, *Phys. Rev. A* **57**, 120 (1998).
- [2] G. Burkard, T. D. Ladd, A. Pan, J. M. Nichol, and J. R. Petta, Semiconductor spin qubits, *Rev. Mod. Phys.* **95**, 025003 (2023).
- [3] P. Stano and D. Loss, Review of performance metrics of spin qubits in gated semiconducting nanostructures, *Nature Reviews Physics* **4**, 672 (2022).
- [4] L. M. K. Vandersypen, H. Bluhm, J. S. Clarke, A. S. Dzurak, R. Ishihara, A. Morello, D. J. Reilly, L. R. Schreiber, and M. Veldhorst, Interfacing spin qubits in quantum dots and donors—hot, dense, and coherent, *npj Quantum Information* **3**, 34 (2017).
- [5] Y. Fang, P. Philippopoulos, D. Culcer, W. A. Coish, and S. Chesi, Recent advances in hole-spin qubits, *Materials for Quantum Technology* **3**, 012003 (2023).
- [6] G. Scappucci, C. Kloeffel, F. A. Zwanenburg, D. Loss, M. Myronov, J.-J. Zhang, S. De Franceschi, G. Katsaros, and M. Veldhorst, The germanium quantum information route, *Nature Reviews Materials* **6**, 926 (2021).
- [7] R. Maurand, X. Jehl, D. Kotekar-Patil, A. Corna, H. Bohuslavskyi, R. Laviéville, L. Hutin, S. Barraud, M. Vinet, M. Sanquer, and S. De Franceschi, A cmos silicon spin qubit, *Nature Communications* **7**, 13575 (2016).
- [8] D. Jirovec, A. Hofmann, A. Ballabio, P. M. Mutter, G. Tavani, M. Botifoll, A. Crippa, J. Kukucka, O. Sagi, F. Martins, J. Saez-Mollejo, I. Prieto, M. Borovkov, J. Arbiol, D. Chrastina, G. Isella, and G. Katsaros, A singlet-triplet hole spin qubit in planar Ge, *Nature Materials* **20**, 1106 (2021).
- [9] P. Steinacker, N. D. Stuyck, W. H. Lim, T. Tanttu, M. Feng, A. Nickl, S. Serrano, M. Candido, J. D. Cifuentes, F. E. Hudson, K. W. Chan, S. Kubicek, J. Jusot, Y. Canvel, S. Beyne, Y. Shimura, R. Loo, C. Godfrin, B. Raes, S. Baudot, D. Wan, A. Laucht, C. H. Yang, A. Saraiva, C. C. Escott, K. D. Greve, and A. S. Dzurak, A 300 mm foundry silicon spin qubit unit cell exceeding 99% fidelity in all operations, [arXiv:2410.15590](https://arxiv.org/abs/2410.15590) (2024).
- [10] S. D. Liles, D. J. Halverson, Z. Wang, A. Shamim, R. S. Eggli, I. K. Jin, J. Hillier, K. Kumar, I. Vorreiter, M. J. Rendell, J. Y. Huang, C. C. Escott, F. E. Hudson, W. H. Lim, D. Culcer, A. S. Dzurak, and A. R. Hamilton, A singlet-triplet hole-spin qubit in mos silicon, *Nature Communications* **15**, 7690 (2024).
- [11] L. C. Camenzind, S. Geyer, A. Fuhrer, R. J. Warburton, D. M. Zumbühl, and A. V. Kuhlmann, A hole spin qubit in a fin field-effect transistor above 4 Kelvin, *Nature Electronics* **5**, 178 (2022).
- [12] S. Geyer, B. Hetényi, S. Bosco, L. C. Camenzind, R. S. Eggli, A. Fuhrer, D. Loss, R. J. Warburton, D. M. Zumbühl, and A. V. Kuhlmann, Anisotropic exchange interaction of two hole-spin qubits, *Nature Physics* **20**, 1152 (2024).
- [13] S. Neyens, O. K. Zietz, T. F. Watson, F. Luthi, A. Nethewala, H. C. George, E. Henry, M. Islam, A. J. Wagner, F. Borjans, E. J. Connors, J. Corrigan, M. J. Curry, D. Keith, R. Kotlyar, L. F. Lampert, M. T. Mądzik, K. Millard, F. A. Mohiyaddin, S. Pellerano, R. Pillarisetty, M. Ramsey, R. Savytskyy, S. Schaal, G. Zheng, J. Ziegler, N. C. Bishop, S. Bojarski, J. Roberts, and J. S. Clarke, Probing single electrons across 300-mm spin qubit wafers, *Nature* **629**, 80 (2024).
- [14] X. Xue, B. Patra, J. P. G. van Dijk, N. Samkharadze, S. Subramanian, A. Corna, B. Paquelet Wuetz, C. Jeon, F. Sheikh, E. Juarez-Hernandez, B. P. Esparza, H. Ramapurawala, B. Carlton, S. Ravikumar, C. Nieva, S. Kim, H.-J. Lee, A. Sammak, G. Scappucci, M. Veldhorst, F. Sebastiano, M. Babaie, S. Pellerano, E. Charbon, and L. M. K. Vandersypen, CMOS-based cryogenic control of silicon quantum circuits, *Nature* **593**, 205 (2021).
- [15] A. M. J. Zwerver, T. Krähenmann, T. F. Watson, L. Lampert, H. C. George, R. Pillarisetty, S. A. Bojarski, P. Amin, S. V. Amitonov, J. M. Boter, R. Caudillo, D. Correas-Serrano, J. P. Dehollain, G. Droulers, E. M. Henry, R. Kotlyar, M. Lodari, F. Lüthi, D. J. Michalak, B. K. Mueller, S. Neyens, J. Roberts, N. Samkharadze, G. Zheng, O. K. Zietz, G. Scappucci, M. Veldhorst, L. M. K. Vandersypen, and J. S. Clarke, Qubits made by advanced semiconductor manufacturing, *Nature Electronics* **5**, 184 (2022).
- [16] T. Kobayashi, J. Salfi, C. Chua, J. van der Heijden, M. G. House, D. Culcer, W. D. Hutchison, B. C. Johnson, J. C. McCallum, H. Riemann, N. V. Abrosimov, P. Becker, H.-J. Pohl, M. Y. Simmons, and S. Rogge, Engineering long spin coherence times of spin-orbit qubits in silicon, *Nature Materials* **20**, 38 (2021).
- [17] N. Piot, B. Brun, V. Schmitt, S. Zihlmann, V. P. Michal,

- A. Apra, J. C. Abadillo-Uriel, X. Jehl, B. Bertrand, H. Niebojewski, L. Hutin, M. Vinet, M. Urdampilleta, T. Meunier, Y.-M. Niquet, R. Maurand, and S. D. Franceschi, A single hole spin with enhanced coherence in natural silicon, *Nature Nanotechnology* **17**, 1072 (2022).
- [18] J. Y. Huang, R. Y. Su, W. H. Lim, M. Feng, B. van Straaten, B. Severin, W. Gilbert, N. Dumoulin Stuyck, T. Tanttu, S. Serrano, J. D. Cifuentes, I. Hansen, A. E. Seedhouse, E. Vahapoglu, R. C. C. Leon, N. V. Abrosimov, H.-J. Pohl, M. L. W. Thewalt, F. E. Hudson, C. C. Escott, N. Ares, S. D. Bartlett, A. Morello, A. Saraiva, A. Laucht, A. S. Dzurak, and C. H. Yang, High-fidelity spin qubit operation and algorithmic initialization above 1 K, *Nature* **627**, 772 (2024).
- [19] S. G. J. Philips, M. T. Madzik, S. V. Amitonov, S. L. de Snoo, M. Russ, N. Kalhor, C. Volk, W. I. L. Lawrie, D. Brouse, L. Tryputen, B. P. Wuetz, A. Sammak, M. Veldhorst, G. Scappucci, and L. M. K. Vandersypen, Universal control of a six-qubit quantum processor in silicon, *Nature* **609**, 919 (2022).
- [20] X. Zhang, E. Morozova, M. Rimbach-Russ, D. Jirovec, T.-K. Hsiao, P. C. Fariña, C.-A. Wang, S. D. Oosterhout, A. Sammak, G. Scappucci, M. Veldhorst, and L. M. K. Vandersypen, Universal control of four singlet-triplet qubits, *Nature Nanotechnology* **20**, 209 (2025).
- [21] N. W. Hendrickx, W. I. L. Lawrie, M. Russ, F. van Riggelen, S. L. de Snoo, R. N. Schouten, A. Sammak, G. Scappucci, and M. Veldhorst, A four-qubit germanium quantum processor, *Nature* **591**, 580 (2021).
- [22] C.-A. Wang, V. John, H. Tidjani, C. X. Yu, A. S. Ivlev, C. Déprez, F. van Riggelen-Doelman, B. D. Woods, N. W. Hendrickx, W. I. L. Lawrie, L. E. A. Stehouwer, S. D. Oosterhout, A. Sammak, M. Friesen, G. Scappucci, S. L. de Snoo, M. Rimbach-Russ, F. Borsoi, and M. Veldhorst, Operating semiconductor quantum processors with hopping spins., *Science* **385**, 447 (2024).
- [23] H. C. George, M. T. Mađzik, E. M. Henry, A. J. Wagner, M. M. Islam, F. Borjans, E. J. Connors, J. Corrigan, M. Curry, M. K. Harper, D. Keith, L. Lampert, F. Luthi, F. A. Mohiyaddin, S. Murcia, R. Nair, R. Nahm, A. Nethewewala, S. Neyens, B. Patra, R. D. Raharjo, C. Rogan, R. Savvitsky, T. F. Watson, J. Ziegler, O. K. Zietz, S. Pellerano, R. Pillarisetty, N. C. Bishop, S. A. Bojarski, J. Roberts, and J. S. Clarke, 12-spin-qubit arrays fabricated on a 300 mm semiconductor manufacturing line, *Nano Letters* **25**, 793 (2025).
- [24] A. Noiri, K. Takeda, T. Nakajima, T. Kobayashi, A. Sammak, G. Scappucci, and S. Tarucha, Fast universal quantum gate above the fault-tolerance threshold in silicon, *Nature* **601**, 338 (2022).
- [25] J. Yoneda, K. Takeda, T. Otsuka, T. Nakajima, M. R. Delbecq, G. Allison, T. Honda, T. Kodera, S. Oda, Y. Hoshi, N. Usami, K. M. Itoh, and S. Tarucha, A quantum-dot spin qubit with coherence limited by charge noise and fidelity higher than 99.9%, *Nature Nanotechnology* **13**, 102 (2018).
- [26] X. Xue, M. Russ, N. Samkharadze, B. Undseth, A. Sammak, G. Scappucci, and L. M. K. Vandersypen, Quantum logic with spin qubits crossing the surface code threshold, *Nature* **601**, 343 (2022).
- [27] W. I. L. Lawrie, M. Russ, F. van Riggelen, N. W. Hendrickx, S. L. de Snoo, A. Sammak, G. Scappucci, and M. Veldhorst, Simultaneous driving of semiconductor spin qubits at the fault-tolerant threshold, [arXiv:2109.07837](https://arxiv.org/abs/2109.07837) (2021).
- [28] A. R. Mills, C. R. Guinn, M. J. Gullans, A. J. Sigillito, M. M. Feldman, E. Nielsen, and J. R. Petta, Two-qubit silicon quantum processor with operation fidelity exceeding 99%, *Science Advances* **8**, eabn5130 (2022).
- [29] A. J. Weinstein, M. D. Reed, A. M. Jones, R. W. Andrews, D. Barnes, J. Z. Blumoff, L. E. Euliss, K. Eng, B. H. Fong, S. D. Ha, D. R. Hulbert, C. A. C. Jackson, M. Jura, T. E. Keating, J. Kerckhoff, A. A. Kiselev, J. Matten, G. Sabbir, A. Smith, J. Wright, M. T. Rakher, T. D. Ladd, and M. G. Borselli, Universal logic with encoded spin qubits in silicon, *Nature* **615**, 817 (2023).
- [30] A. Mills, C. Guinn, M. Feldman, A. Sigillito, M. Gullans, M. Rakher, J. Kerckhoff, C. Jackson, and J. Petta, High-fidelity state preparation, quantum control, and readout of an isotopically enriched silicon spin qubit, *Phys. Rev. Appl.* **18**, 064028 (2022).
- [31] T. Kobayashi, T. Nakajima, K. Takeda, A. Noiri, J. Yoneda, and S. Tarucha, Feedback-based active reset of a spin qubit in silicon, *npj Quantum Information* **9**, 52 (2023).
- [32] K. Takeda, A. Noiri, T. Nakajima, L. C. Camenzind, T. Kobayashi, A. Sammak, G. Scappucci, and S. Tarucha, Rapid single-shot parity spin readout in a silicon double quantum dot with fidelity exceeding 99%, *npj Quantum Information* **10**, 22 (2024).
- [33] M. D. Michielis, E. Ferraro, E. Prati, L. Hutin, B. Bertrand, E. Charbon, D. J. Ibberson, and M. F. Gonzalez-Zalba, Silicon spin qubits from laboratory to industry, *Journal of Physics D: Applied Physics* **56**, 363001 (2023).
- [34] A. Saraiva, W. H. Lim, C. H. Yang, C. C. Escott, A. Laucht, and A. S. Dzurak, Materials for silicon quantum dots and their impact on electron spin qubits, *Advanced Functional Materials* **32**, 2105488 (2022).
- [35] L. Bellentani, M. Bina, S. Bonen, A. Secchi, A. Bertoni, S. P. Voinigescu, A. Padovani, L. Larcher, and F. Troiani, Toward hole-spin qubits in Si *p*-MOSFETs within a planar CMOS foundry technology, *Phys. Rev. Applied* **16**, 054034 (2021).
- [36] L. Petit, M. Russ, G. H. G. J. Eenink, W. I. L. Lawrie, J. S. Clarke, L. M. K. Vandersypen, and M. Veldhorst, Design and integration of single-qubit rotations and two-qubit gates in silicon above one Kelvin, *Communications Materials* **3**, 82 (2022).
- [37] D. V. Bulaev and D. Loss, Spin relaxation and decoherence of holes in quantum dots, *Phys. Rev. Lett.* **95**, 076805 (2005).
- [38] D. V. Bulaev and D. Loss, Electric dipole spin resonance for heavy holes in quantum dots, *Phys. Rev. Lett.* **98**, 097202 (2007).
- [39] S. Bosco, B. Hetényi, and D. Loss, Hole spin qubits in Si FinFETs with fully tunable spin-orbit coupling and sweet spots for charge noise, *PRX Quantum* **2**, 010348 (2021).
- [40] S. Bosco, M. Benito, C. Adelsberger, and D. Loss, Squeezed hole spin qubits in Ge quantum dots with ultrafast gates at low power, *Phys. Rev. B* **104**, 115425 (2021).
- [41] S. D. Liles, F. Martins, D. S. Miserev, A. A. Kiselev, I. D. Thorvaldson, M. J. Rendell, I. K. Jin, F. E. Hudson, M. Veldhorst, K. M. Itoh, O. P. Sushkov, T. D. Ladd, A. S. Dzurak, and A. R. Hamilton, Electrical control of the *g* tensor of the first hole in a silicon MOS quantum

- dot, *Phys. Rev. B* **104**, 235303 (2021).
- [42] V. P. Michal, B. Venitucci, and Y.-M. Niquet, Longitudinal and transverse electric field manipulation of hole spin-orbit qubits in one-dimensional channels, *Phys. Rev. B* **103**, 045305 (2021).
- [43] V. John, F. Borsoi, Z. György, C.-A. Wang, G. Széchenyi, F. van Riggelen-Doelman, W. I. L. Lawrie, N. W. Hendrickx, A. Sammak, G. Scappucci, A. Pályi, and M. Veldhorst, Bichromatic Rabi control of semiconductor qubits, *Phys. Rev. Lett.* **132**, 067001 (2024).
- [44] S. Bosco, S. Geyer, L. C. Camenzind, R. S. Egli, A. Fuhrer, R. J. Warburton, D. M. Zumbühl, J. C. Egues, A. V. Kuhlmann, and D. Loss, Phase-driving hole spin qubits, *Phys. Rev. Lett.* **131**, 197001 (2023).
- [45] M. J. Carballido, S. Svab, R. S. Egli, T. Patlatiuk, P. C. Kwon, J. Schuff, R. M. Kaiser, L. C. Camenzind, A. Li, N. Ares, E. P. A. M. Bakkers, S. Bosco, J. C. Egues, D. Loss, and D. M. Zumbühl, Compromise-free scaling of qubit speed and coherence, [arXiv:2402.07313](https://arxiv.org/abs/2402.07313) (2024).
- [46] C. Kloeffel, M. J. Rančić, and D. Loss, Direct rashba spin-orbit interaction in Si and Ge nanowires with different growth directions, *Phys. Rev. B* **97**, 235422 (2018).
- [47] C. Adelsberger, M. Benito, S. Bosco, J. Klinovaja, and D. Loss, Hole-spin qubits in Ge nanowire quantum dots: Interplay of orbital magnetic field, strain, and growth direction, *Phys. Rev. B* **105**, 075308 (2022).
- [48] J. C. Abadillo-Uriel, E. A. Rodríguez-Mena, B. Martínez, and Y.-M. Niquet, Hole-spin driving by strain-induced spin-orbit interactions, *Phys. Rev. Lett.* **131**, 097002 (2023).
- [49] J. Fischer, W. A. Coish, D. V. Bulaev, and D. Loss, Spin decoherence of a heavy hole coupled to nuclear spins in a quantum dot, *Phys. Rev. B* **78**, 155329 (2008).
- [50] S. Bosco and D. Loss, Fully tunable hyperfine interactions of hole spin qubits in Si and Ge quantum dots, *Phys. Rev. Lett.* **127**, 190501 (2021).
- [51] L. Cvitkovich, P. Stano, C. Wilhelmer, D. Waldhör, D. Loss, Y.-M. Niquet, and T. Grasser, Coherence limit due to hyperfine interaction with nuclei in the barrier material of Si spin qubits, *Phys. Rev. Appl.* **22**, 064089 (2024).
- [52] B. Venitucci, L. Bourdet, D. Pouzada, and Y.-M. Niquet, Electrical manipulation of semiconductor spin qubits within the  $g$ -matrix formalism, *Phys. Rev. B* **98**, 155319 (2018).
- [53] A. Secchi, L. Bellentani, A. Bertoni, and F. Troiani, Interacting holes in Si and Ge double quantum dots: From a multiband approach to an effective-spin picture, *Phys. Rev. B* **104**, 035302 (2021).
- [54] P. Stano and D. Loss, Quantification of the heavy-hole–light-hole mixing in two-dimensional hole gases, *Phys. Rev. B* **111**, 115301 (2025).
- [55] N. Ares, V. N. Golovach, G. Katsaros, M. Stoffel, F. Fournel, L. I. Glazman, O. G. Schmidt, and S. De Franceschi, Nature of tunable hole  $g$  factors in quantum dots, *Phys. Rev. Lett.* **110**, 046602 (2013).
- [56] G. Forghieri, A. Secchi, A. Bertoni, P. Bordone, and F. Troiani, Quantum estimation and remote charge sensing with a hole-spin qubit in silicon, *Phys. Rev. Res.* **5**, 043159 (2023).
- [57] O. Malkoc, P. Stano, and D. Loss, Charge-noise-induced dephasing in silicon hole-spin qubits, *Phys. Rev. Lett.* **129**, 247701 (2022).
- [58] C.-A. Wang, H. E. Ercan, M. F. Gyure, G. Scappucci, M. Veldhorst, and M. Rimbach-Russ, Modeling of planar germanium hole qubits in electric and magnetic fields, *npj Quantum Information* **10**, 102 (2024).
- [59] B. Hetényi, S. Bosco, and D. Loss, Anomalous zero-field splitting for hole spin qubits in Si and Ge quantum dots, *Phys. Rev. Lett.* **129**, 116805 (2022).
- [60] P. M. Mutter and G. Burkard, All-electrical control of hole singlet-triplet spin qubits at low-leakage points, *Phys. Rev. B* **104**, 195421 (2021).
- [61] D. Jirovec, P. M. Mutter, A. Hofmann, A. Crippa, M. Rychetsky, D. L. Craig, J. Kukucka, F. Martins, A. Ballabio, N. Ares, D. Chrastina, G. Isella, G. Burkard, and G. Katsaros, Dynamics of hole singlet-triplet qubits with large  $g$ -factor differences, *Phys. Rev. Lett.* **128**, 126803 (2022).
- [62] D. Fernández-Fernández, Y. Ban, and G. Platero, Quantum control of hole spin qubits in double quantum dots, *Phys. Rev. Appl.* **18**, 054090 (2022).
- [63] J. Saez-Mollejo, D. Jirovec, Y. Schell, J. Kukucka, S. Calcaterra, D. Chrastina, G. Isella, M. Rimbach-Russ, S. Bosco, and G. Katsaros, Exchange anisotropies in microwave-driven singlet-triplet qubits, [arXiv:2408.03224](https://arxiv.org/abs/2408.03224) (2024).
- [64] S. Bosco and M. Rimbach-Russ, [Exchange-only spin-orbit qubits in silicon and germanium](https://arxiv.org/abs/2410.05461) (2024), [arXiv:2410.05461](https://arxiv.org/abs/2410.05461) [cond-mat.mes-hall].
- [65] W. I. L. Lawrie, N. W. Hendrickx, F. van Riggelen, M. Russ, L. Petit, A. Sammak, G. Scappucci, and M. Veldhorst, Spin relaxation benchmarks and individual qubit addressability for holes in quantum dots, *Nano Letters* **20**, 7237 (2020).
- [66] B. Voisin, R. Maurand, S. Barraud, M. Vinet, X. Jehl, M. Sanquer, J. Renard, and S. De Franceschi, Electrical control of  $g$ -factor in a few-hole silicon nanowire MOSFET, *Nano Letters* **16**, 88 (2016).
- [67] H. Liu, T. Zhang, K. Wang, F. Gao, G. Xu, X. Zhang, S.-X. Li, G. Cao, T. Wang, J. Zhang, X. Hu, H.-O. Li, and G.-P. Guo, Gate-tunable spin-orbit coupling in a germanium hole double quantum dot, *Physical Review Applied* **17**, 044052 (2022).
- [68] V. John, C. X. Yu, B. van Straaten, E. A. Rodríguez-Mena, M. Rodríguez, S. D. Oosterhout, L. E. A. Stehouwer, G. Scappucci, M. Rimbach-Russ, S. Bosco, F. Borsoi, Y.-M. Niquet, and M. Veldhorst, Robust and localised control of a 10-spin qubit array in germanium, *Nature Communications* **16**, 10560 (2025).
- [69] V. John, C. X. Yu, B. van Straaten, E. A. Rodríguez-Mena, M. Rodríguez, S. Oosterhout, L. E. A. Stehouwer, G. Scappucci, S. Bosco, M. Rimbach-Russ, Y.-M. Niquet, F. Borsoi, and M. Veldhorst, A two-dimensional 10-qubit array in germanium with robust and localised qubit control, [arXiv:2412.16044](https://arxiv.org/abs/2412.16044) (2025).
- [70] F. De Palma, F. Oppliger, W. Jang, S. Bosco, M. Janík, S. Calcaterra, G. Katsaros, G. Isella, D. Loss, and P. Scarlino, Strong hole-photon coupling in planar Ge for probing charge degree and strongly correlated states, *Nature Communications* **15**, 10177 (2024).
- [71] J. M. Luttinger and W. Kohn, Motion of electrons and holes in perturbed periodic fields, *Phys. Rev.* **97**, 869 (1955).
- [72] L. C. L. Y. Voon and M. Willatzen, *The  $kp$  Method* (Springer Berlin, 2009).
- [73] L. A. Terrazos, E. Marcellina, Z. Wang, S. N. Copper-smith, M. Friesen, A. R. Hamilton, X. Hu, B. Koiller,

- A. L. Saraiva, D. Culcer, and R. B. Capaz, Theory of hole-spin qubits in strained germanium quantum dots, *Phys. Rev. B* **103**, 125201 (2021).
- [74] C. David Sherrill and H. F. Schaefer, The configuration interaction method: Advances in highly correlated approaches (Academic Press, 1999) pp. 143–269.
- [75] A. Secchi, L. Bellentani, A. Bertoni, and F. Troiani, Inter- and intraband Coulomb interactions between holes in silicon nanostructures, *Phys. Rev. B* **104**, 205409 (2021).
- [76] See the Supplemental Material at ... for further details on: Luttinger-Kohn Hamiltonian (with Bir-Pikus terms); single- and three-hole states calculation; classical equilibrium configurations of the three-hole states.
- [77] E. Fanucchi, G. Forghieri, A. Secchi, P. Bordone, and F. Troiani, Giant Rabi frequencies between qubit and excited hole states in silicon quantum dots, *Phys. Rev. B* **111**, 205409 (2025).
- [78] G. L. Bir and G. E. Pikus, *Symmetry and strain-induced effects in semiconductors* (Wiley, 1974).
- [79] C. Y.-P. Chao and S. L. Chuang, Spin-orbit-coupling effects on the valence-band structure of strained semiconductor quantum wells, *Phys. Rev. B* **46**, 4110 (1992).
- [80] A. Secchi and F. Troiani, Envelope-function theory of inhomogeneous strain in semiconductor nanostructures, *Phys. Rev. B* **110**, 045420 (2024).
- [81] V. Sverdlov, *Strain-Induced Effects in Advanced MOS-FETs* (Springer, 2011).
- [82] A. Sammak, D. Sabbagh, N. W. Hendrickx, M. Lodari, B. Paquelet Wuetz, A. Tosato, L. Yeoh, M. Bollani, M. Virgilio, M. A. Schubert, P. Zaumseil, G. Capellini, M. Veldhorst, and G. Scappucci, Shallow and undoped germanium quantum wells: A playground for spin and hybrid quantum technology, *Advanced Functional Materials* **29**, 1807613 (2019).